Combining the Perspective of Satellite- and Ground-Based Observations to Analyze Cloud Frontal Systems

ANJA HÜNERBEIN, HARTWIG DENEKE, AND ANDREAS MACKE

Leibniz Institute for Tropospheric Research, Leipzig, Germany

KERSTIN EBELL

Institute for Geophysics and Meteorology, University of Cologne, Cologne, Germany

ULRICH GÖRSDORF

Meteorologisches Observatorium Lindenberg, German Weather Service, Lindenberg, Germany

(Manuscript received 28 August 2013, in final form 30 June 2014)

ABSTRACT

A method is presented to analyze the cloud life cycle of frontal systems passing over European supersites. It combines information on the vertical profiles of cloud properties derived from ground-based observations with cloud products obtained from satellite-based observations, including their spatial variability. The Euler and Lagrange perspectives are adopted to consider the history of a cloud system that passes the supersites. The forward model known as RTTOV (Radiative Transfer for the Television and Infrared Observation Satellite Operational Vertical Sounder) and the ground-based ''CloudNET'' products are used to simulate synthetic satellite observations at the supersites, which are subsequently compared with the actual observations of the Meteosat Spinning Enhanced Visible and Infrared Imager (SEVIRI) instrument. Different metrics are considered to quantify and interpret the consistency of the synthetic and the observed satellite data: brightness temperatures at the thermal IR channels, the split-window channels, and trispectral combinations, as well as the outgoing longwave radiation. In this way, the uncertainties of the individual datasets are investigated. This knowledge provides the motivation to combine the disjunct cloud products from satellite with those from ground instruments to characterize the development of the passing cloud frontal systems. In addition, back trajectories started at different stages of the cloud system were used to analyze its history prior to the supersite overpass. The trajectories are used to study, for example, the life time of the cloud frontal system, changes of the cloud phase, and the evolution of cloud physics such as optical thickness, effective particle size, and water path. As a test bed, a case study with a cold front passing Lindenberg, Germany, is presented.

1. Introduction

Midlatitude cyclones are everyday phenomena of the weather in the midlatitudes. Together with anticyclones, they are responsible for the meridional transport of energy. The cloud systems associated with midlatitude cyclones have been the subject of extensive studies to improve their synoptic understanding and weather prediction. The first conceptual model was introduced by Bjerknes (1919), followed by several enhancements to the understanding of cyclogenesis [e.g., see review by Shapiro and Grønås (1999)]. Together with the development of numerical models, the observation of cloud parameters from the ground and from space plays an important role in improving our understanding of the governing processes. A set of prior studies has used satellite cloud observations such as cloud cover, cloud-top height (CTH), and cloud optical thickness (COT) to analyze cloud distribution, structure, and precipitation in midlatitude cyclones to assess general circulation

Denotes Open Access content.

Corresponding author address: Anja Hünerbein, Leibniz Institute for Tropospheric Research, Permoserstraße 15, 04318 Leipzig, Germany.
E-mail: anjah@tropos.de

DOI: 10.1175/JAMC-D-13-0274.1

models (Jakob 2003; Field and Wood 2007; Field et al. 2008). With the launch of a cloud radar on *CloudSat* (Stephens et al. 2002) and a cloud–aerosol lidar on *Cloud–Aerosol Lidar and Infrared Pathfinder Satellite Observations* (*CALIPSO*; Winker et al. 2009), the capabilities have been enhanced to also provide vertical profiles of cloud properties across cloud frontal systems from space. The three-dimensional cloud distributions from the polar orbiter's track have been used to verify conceptual models as well as to evaluate the physical parameterizations in general circulation models (Field et al. 2011; Naud et al. 2010). In recent years, different ground stations, that is, so-called supersites, have been established to continuously monitor clouds using a suite of remote sensing instruments. These supersites enable a comprehensive view of the vertical structure of cloud properties. The first supersite was established in the framework of the Atmospheric Radiation Measurement Program (ARM; Stokes and Schwartz 1994) that is funded by the U.S. Department of Energy. In Europe, a number of supersites have been established under the umbrella of the ''CloudNET'' project (Illingworth et al. 2007), which are consolidated by the European Aerosols, Clouds, and Trace Gases Research InfraStructure Network (ACTRIS; http://www.actris.net). At these stations, the synergy of cloud radar, lidar, and microwave radiometer is exploited to continuously provide data products of cloud properties. The number of these high-quality measurement sites will, however, always remain insufficient to fully capture the spatial variation and the different states of a cloud system because of the point nature of the observations.

In this study, we propose a method to combine ground-based measurements with geostationary satellite observations from the Spinning Enhanced Visible and Infrared Imager (SEVIRI) instrument over Europe for a comprehensive view on frontal cloud systems. The surface sites provide Eulerian time series of parameters of the passing cloud systems with high vertical resolution, and the passive remotely sensed products from the geostationary satellite offer temporally and also horizontally resolved views of the cloud fields. In addition, we employ back trajectories together with the geostationary satellite product to investigate the temporal evolution, that is, the history, of the cloud systems. Thereby we are able to analyze clouds as a four-dimensional object.

First attempts to integrate satellite and ground observations have been made by Feijt and van Lammeren (1996) and van Lammeren et al. (2000). In more recent studies, ground-based measurements are used to validate the products from Meteosat SEVIRI, for example, the cloud liquid water path (LWP) (Roebeling et al. 2008; Greuell and Roebeling 2009).

The main challenge of the combination is to understand and quantify the discrepancies between the two perspectives. By means of the Radiative Transfer for the Television and Infrared Observation Satellite Operational Vertical Sounder (RTTOV; Eyre 1991) model used as a satellite forward operator, we relate the retrieved cloud-property profiles at the supersites to synthetic satellite data. The forward-model approach gives us the top-of-atmosphere satellite radiances with uncertainties that are based on the point measurements. The different spatial and time scales of the synthetic satellite radiances and those observed by the Meteosat SEVIRI instrument are taken into account by following the approach of previous studies (Roebeling et al. 2008; Greuell and Roebeling 2009, their section 2). We consider different metrics to quantify and interpret the consistency of the synthetic and observed satellite data: brightness temperatures (BTs) at the thermal IR channels, the split-window channels, and trispectral combinations, as well as the outgoing longwave radiation. We are confident in combining the two perspectives if the observed satellite data can be reproduced within the uncertainties of all metrics. For those times when the consistency check has been passed, we study the accuracy and precision of the cloud products that are retrieved from both perspectives such as CTH and cloud water path (CWP). Further, we combine the complement cloud products from the satellite with ground measurements to characterize the passing cloud frontal systems over the sites. Back trajectories for different cloud states started at the supersites are utilized in conjunction with the satellite cloud products to gain a better understanding of relevant cloud processes, including the cloud life cycle, the onset of precipitation, and the microphysical development. The focus of the paper is the description of the developed method, that is, a consistency check to combine the ground-based and satellite observations and the characterization of the cloud frontal systems via the Euler (cloud systems passing over the sites) and Lagrange (cloud tracking) perspectives. An example—that is, the passage of a cloud frontal system at the supersite Lindenberg—is analyzed to demonstrate this approach.

The outline of this paper is as follows. In section 2 the satellite- and ground-based measurements and retrieved products are described. The method to analyze the cloud life time by combining the different observations is introduced in section 3. In section 4, the performance of the method is shown for a case study. A summary is given and conclusions are drawn in section 5.

2. Measurements

a. Satellite-based observations

The SEVIRI (Schmetz et al. 2002) instruments are operated by the European Organisation for the Exploitation of Meteorological Satellites (EUMETSAT) and fly on board the second generation of Meteosat satellites (MSG). SEVIRI is a scanning radiometer with 12 spectral channels in the visible, near-infrared, and thermal infrared spectral regions. At nadir, the spatial resolution is 3 km × 3 km for the narrowband channels and 1 km × 1 km for the high-resolution broadband visible channel. For the former, the sampling pixel size at the ground station Lindenberg, Germany, that is considered in this study is 6.6 km (north–south) × 3.4 km (east–west). The full Earth view is scanned every 15 min by the primary geostationary 0° longitude service. The upper one-third of Earth is scanned every 5 min by a second MSG satellite at 9.5°E operating in the so-called Rapid Scan Service. This last mode covers Europe and allows the continuous study of the daily cycle of weather patterns at unrepresented temporal resolution from space. In this study, the thermal IR channels, that is, 6.2, 7.3, 8.7, 9.7, 10.8, 12.0, and 13.4 μm, build the basis for a comparison with simulated synthetic satellite data. The synthetic satellite data are created by forward modeling, using the vertical-profile information from the ground-based measurements as input to the RTTOV model. The different thermal IR channels provide different information, for example, on the water-vapor distribution (6.2 and 7.3 μm); temperature of the clouds, land, and sea surface (8.7, 10.8, and 12.0 μm); or the atmospheric air mass (9.7 and 13.4 μm). The outgoing longwave radiation (OLR) is used as an additional metric to quantify the spectral information. It is calculated from the synthetic and observed satellite data using a regression scheme (EUMETSAT 2014). We indirectly make use of the visible and near-infrared channels, since they are input to the cloud physical properties (CPP) algorithm used in this study. The CPP algorithm has been developed at the Royal Netherlands Meteorological Institute (KNMI; Roebeling et al. 2006) within the scope of the satellite application facility on climate monitoring (Schulz et al. 2009). The CPP product provides estimates of COT, cloud particle sizes (REF), and CWP, which are derived from the reflectances at the visible and near-infrared SEVIRI channels by using the Nakajima and King (1990) method. CWP represents the amount of the column-integrated cloud liquid and ice water and is calculated from COT and REF values according to the formula by Stephens (1978). The Nowcasting Satellite Application Facilities (NWC SAF) cloud products are utilized to identify whether a SEVIRI pixel is cloudy, cloud free, or snow/ice contaminated as well as to infer the CTH (Derrien 2013). The error sources for the satellite values of CWP and CTH have been discussed and analyzed in several studies: In general, cloud remote sensing techniques rely on the assumption of a plane-parallel and homogeneous cloud, which causes considerable uncertainties in the retrieval of cloud properties. Zinner and Mayer (2006) have quantified the uncertainties with three-dimensional Monte Carlo radiative transfer calculations for marine stratocumulus clouds. If the pixels are completely covered by clouds, then the biases are less than ±5%, but partially covered pixels can cause an underestimation of up to 20% and more. Validation of cloud properties from SEVIRI against ground-based measurements has revealed a bias of 15% (Roebeling et al. 2008; Greuell and Roebeling 2009) for the LWP and 0.12 km for the CTH of opaque clouds (Derrien 2012).

b. Ground-based observations

The ground-based dataset used in this study is a synergistic product of cloud radar, ceilometer, and multifrequency microwave radiometer (MWR) measurements. This product is derived for observation sites such as Jülich, Germany (Jülich Observatory for Cloud Evolution, or JOYCE); Leipzig, Germany (Leipzig Aerosol and Cloud Remote Observations System, or LACROS); and Lindenberg (Meteorologisches Observatorium Lindenberg, or MOL) by using the retrieval package that was developed in the CloudNET project (Illingworth et al. 2007). Data are available (24 hours per day for 7 days per week) with a temporal and vertical resolution of 30 s and 60 m, respectively. Note that the CloudNET retrievals provide information on the entire vertical extent of clouds. In the first step, a target classification including the determination of cloud base and top is performed from the radar profiles of reflectivity, Doppler velocity, ceilometer backscatter profiles, as well as temperature and humidity profiles provided by a numerical weather prediction model [e.g., the Germany-focused Consortium for Small-Scale Modeling (COSMO-DE) model for the Lindenberg site] or radiosounding. Microphysical parameters are derived subsequently. The profile of liquid water content (LWC) is estimated by calculating the theoretical adiabatic LWC gradient for each liquid water cloud layer (Albrecht et al. 1990; Boers et al. 2000). The integrated LWC values are finally scaled to the MWR measured LWP. The ice water content (IWC) is calculated as a function of radar reflectivity and temperature (Hogan et al. 2006). This empirical formula has been derived on the basis of a large midlatitude aircraft dataset. The estimated random and systematic errors of LWC and IWC result from the uncertainty of the microwave radiometer LWP retrieval as well as from the

uncertainty in cloud base and random error in radar reflectivity factor, respectively.

3. Methods

a. Combining satellite- and ground-based observations

1) FORWARD MODEL (RTTOV)

The vertical profiles of IWC and LWC retrieved from the ground-based measurements are the input for the RTTOV forward model to simulate the infrared SEVIRI radiances. For the forward calculation, the cloud cover is set to 1 for those profile layers for which the IWC or LWC values are greater than zero. Vertical profiles of temperature and humidity are used from the COSMO-DE forecast model because it also has been utilized to retrieve the CloudNET products. The CloudNET products also provide estimated errors of LWC and IWC, which have been used to determine the uncertainty in the synthetic satellite data. The simulation is performed with RTTOV, version 9.3 (v9.3), a fast radiative transfer model. A detailed description of the RTTOV model can be found in Eyre (1991) and Saunders et al. (1999, 2010). The optical parameters for water clouds are available for five size distributions corresponding to five different water cloud types (stratus continental, stratus maritime, cumulus continental clean, cumulus continental polluted, and cumulus maritime). In this study, we set the water cloud, an altocumulus cloud, to the cumulus continental clean type. For ice clouds, one ice cloud type is available with four different ice cloud parameterizations and two ice crystal shapes. The ice parameterizations have been evaluated with the collocated satellite and aircraft measurements from the Cirrus Cloud Experiment (CIRCLE-2; J. Vidot 2011, personal communication). Since the aggregate type as ice crystal shape has shown best results in the evaluation study by J. Vidot (2011, personal communication), we used this ice shape together with the parameterization of McFarquhar et al. (2003) in the RTTOV simulations. The background aerosol is assumed to be of the type "continental clean." Aerosol has only a minor influence on the calculations of the SEVIRI BTs, however, because of the small effect in the infrared. The surface emissivity used is based on the Moderate Resolution Imaging Spectroradiometer (MODIS) surface emissivity product ("MOD11C3") for the 8.5-, 10.8-, and 12.0-μm SEVIRI channels. For the remaining channels, the surface emissivity is calculated by assuming the spectral dependency of the emissivity for vegetation from the MODIS University of California, Santa Barbara, emissivity library (Wan et al. 1994).

2) PREPARATION OF THE SYNTHETIC AND MEASURED SATELLITE OBSERVATIONS

The differences between the time and length scales for the satellite- and ground-based observations as well as the synthetic satellite observations have to be considered to match the diverse perspectives. The time series (all 30 s) measured and simulated at a single point (the ground station) can be interpreted as spatial variation passed along with the Eulerian mean flow (frozen turbulent hypothesis; Taylor 1938). This assumes that the advection velocity of the airflow is much greater than the velocity scale of the turbulence itself. Especially for small cumulus clouds that fall below the SEVIRI pixel resolution, the error introduced by the frozen-turbulence assumption will increase (Higgins et al. 2012). In previous studies, the applicability of this assumption has been analyzed with respect to the comparability of ground-based or satellite-based statistics from vertical profile measurements to spatial statistics using global circulation models (Grützun et al. 2013; Astin et al. 2001; Bouniol et al. 2010). On the basis of a model study, Grützun et al. (2013) have shown that higher-order moments of the humidity distribution do not compare well. We do not have the knowledge of the cloud fraction within a SEVIRI pixel. Therefore, we have been focused on large cloud systems such as cloud frontal systems to reduce the problems with subpixel cloud variability. In Greuell and Roebeling (2009), different strategies to evaluate ground and satellite measurements have been assessed with respect to the LWP of relatively low clouds (lower than 3 km). They found optimal validation methods by averaging with a Gaussian weight function in space and time domains. The length of the temporal averaging of the ground-based measurements should conform to the time the cloud needs to move over the corresponding satellite footprint. Deneke et al. (2009) suggests a value of even 6 times as large as this time. Assuming a mean wind speed of 10 m s^{-1} at cloud top, a temporal average of 15 min results in a 9-km track length, which is representative for one SEVIRI pixel. Therefore we used a moving average of 15 min for the simulated SEVIRI observations. This value could be refined if the vertical wind profile was available. In this way we keep the high temporal frequency of the ground-based measurements (30 s) and build the bridge to the observed satellite data time scale. We selected the same time stamp for the comparison with the satellite measurements, which are available every 5 min. The satellite pixel has been collocated to the ground station. A mismatch error can be caused by slight misallocation of the ground station relative to the center of the field of view (FOV) of the SEVIRI pixel (see Fig. 1) or the incorrect

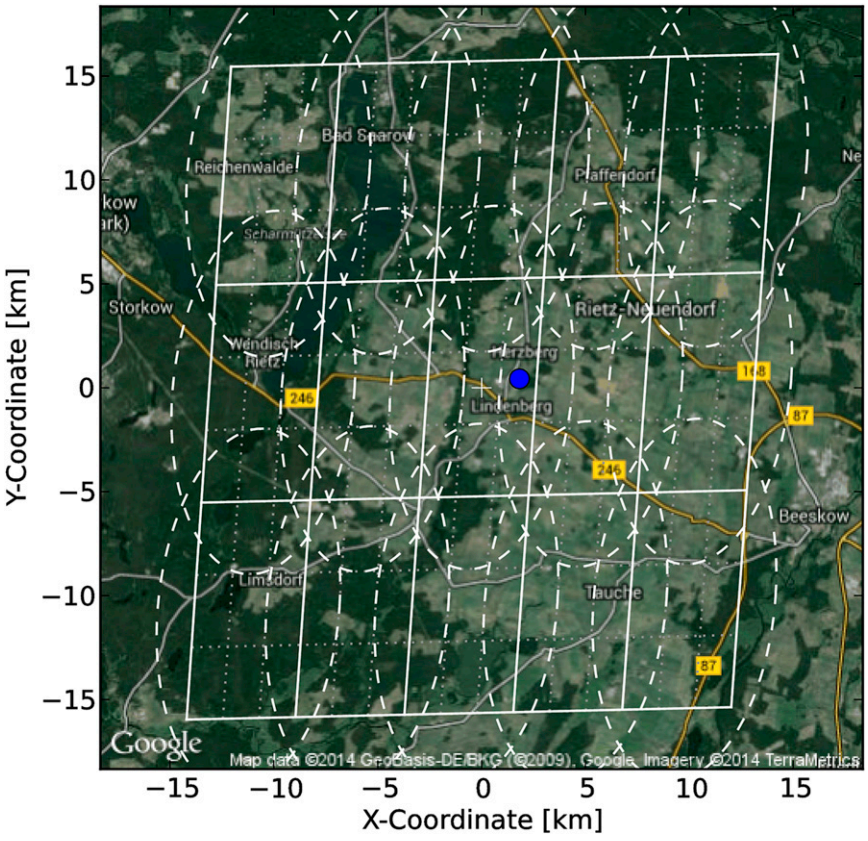

FIG. 1. Google map of Lindenberg in Mercator projection as used for the Google Maps service (EPSG:3857), showing the 5 × 3 pixel grid of Meteosat SEVIRI pixels used in our analysis as overlay (solid white lines). In addition, the true optical resolution of the SEVIRI instrument is indicated (dashed lines) as well as the corresponding grid of high-resolution-visible-channel pixels (dotted lines). The Lindenberg observatory is marked by the blue point. The background map data are copyright 2014 Geobasis DE/BKG (copyright 2009); Google Imagery are copyright 2014 TerraMetrics.

attribution of clouds to a certain altitude, for example. SEVIRI views Earth at an oblique angle, the satellite zenith angle θ_s. This implies that a cloud that is located directly above a ground-based site is displaced (Displ) in the SEVIRI pixel. This parallax effect can be corrected if the cloud-top height H and θ_s are known (Fig. 4 in Greuell and Roebeling 2009):

$$\text{Displ} = H \tan\theta_s .$$

At Lindenberg, θ_s is 61.05°. Thus, for a typical CTH in a frontal system, for example, 10 km, the displacement is to the north by almost 20 km northeast of Lindenberg. Furthermore, note that the FOV of the SEVIRI instrument is several orders of magnitude larger than the FOV of the ground-based instrumentation. The uncertainty related to the different observing geometries has been taken into account in the analysis in terms of the spatial variability of the satellite measurements. To this end, the standard deviation of the SEVIRI BTs of the 5 × 3 pixels surrounding the corresponding supersite has been calculated at each observation time, which takes into account the elongated shape of the SEVIRI pixel that is due to the steep viewing angle for the European stations (Fig. 1). This number provides information on the horizontal homogeneity/inhomogeneity of the observed scene. In summary, to consider the uncertainty of the spatial collocation of the satellite pixel to the ground station, we have used not only the parallax corrected pixel but also the surrounding 5 × 3 pixels (Fig. 1).

b. *Calculation of the back trajectories*

To describe the history of the cloud systems, that is, the development of its microphysical properties, we assume that the frontal system moves with the air mass. The back trajectory of the air mass is determined by a Lagrangian particle dispersion model, "FLEXPART" (Stohl et al. 2005). FLEXPART has been developed at

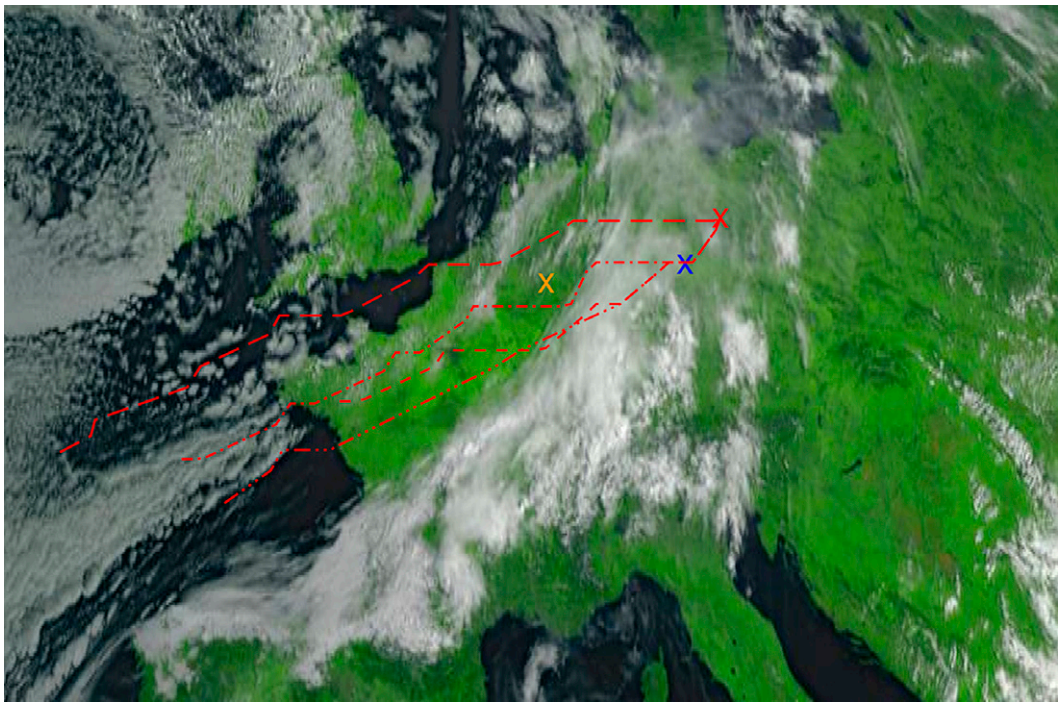

FIG. 2. SEVIRI true-color image at 0800 UTC 12 May 2011, with the back trajectories started at 0000 (long dashes), 0600 (dash–dots), 1200 (dash–dot–dot–dots), and 1800 (short dashes) UTC as well as the supersites Lindenberg (red X), Leipzig (blue X), and Jülich (orange X).

the Norwegian Institute for Air Research and has been used for a variety of research studies. FLEXPART operates on a terrain-following Cartesian coordinate system and accounts for particle transport and diffusion as well as removal processes, that is, wet or dry deposition. The backward simulation is initiated with 50 000 particles, which are infinitesimal small parcels of air. The release point has been set to the height of the cloud layer at Lindenberg on 12 May 2011 at 0000, 0006, 1200, and 1800 UTC. The backward simulation of the transport of the air particle is based on 3D temperature, specific humidity, mass flux, and wind fields from the forecast system reanalysis that is managed by the National Centers for Environmental Prediction. The reanalysis data have a temporal resolution of 6 h and a horizontal resolution of $1° \times 1°$. The model output provides the concentration of the tracked air particles, that is, particle density, in four dimensions: on a longitude, latitude, and height grid and with a temporal resolution of 2 h. The concentration field has been integrated over the height to get a three-dimensional field. Then, the coordinates (longitude and latitude) have been calculated by finding the maximum concentration of the tracked air particles for each time step. During the first day, the density distribution of the concentration is compact and no ambiguous solutions are found. Last, we get one coordinate for each time step, which results in the back trajectory (see Fig. 2). For each time step, we applied nearest-neighbor interpolation in space and time to find the corresponding satellite coordinate along the back trajectory.

4. Results of a case study

The method described in the previous section has been applied to a case study that is a cold-frontal passage over Europe on 12 May 2011 (Fig. 2). This cold front belongs to a low pressure system over the North Atlantic Ocean moving from west to east. The corresponding band of clouds went from southern Scandinavia over central Germany to the Bay of Biscay. Frontal waves built up on the cold front and slowed down the motion of the frontal system. The circulation weather type of this frontal system is found to be a cyclonic circulation with southwesterly airflow. Note that the analysis could be easily extended to the observations of the other supersites JOYCE and LACROS, which also nicely captured the passage of the frontal system. To illustrate the method presented in section 3, we focus on the Lindenberg site.

a. Combining satellite- and ground-based observation: A consistency check

To obtain synthetic satellite data over Lindenberg, a forward simulation for the cold-frontal system that passed Lindenberg has been performed using the

RTTOV model. RTTOV was run from 0000 to 0000 UTC (24 h) with a time step of 30 s, defined by the CloudNET cloud products and with the thermodynamic profiles provided by the COSMO-DE model. We have further simulated the uncertainties of synthetic satellite data due to the given error of the LWC and IWC CloudNET products. The moving average and the parallax correction have been applied to synthetic and observed satellite data as described in section 3. The uncertainty of the horizontal homogeneity/inhomogeneity of the observed satellite data is given by the standard deviation of the 5×3 pixels surrounding the parallax-corrected pixel. To quantify and interpret the consistency of the synthetic and the observed satellite data we have considered different metrics: the brightness temperatures at the thermal IR channels, the split-window channels, and trispectral combination of channels as well as the OLR. The requirement for the consistency check should be to fulfill the comparison within the calculated error bars.

Figure 3 shows the comparison of the observed and synthetic BTs for the two water-vapor channels (6.2 and 7.3 μm), the window channels (8.7, 10.8 and 12.0 μm), and channel combinations, respectively, as well as the OLR. Note that the BT scale is inverted in the plots showing the time series to better indicate the height of the clouds. Most of the time, the simulated BTs agree well with the observed ones and are within the error bars. Thus they comply with the requirements. The uncertainties in the synthetic satellite data are lowest for the water-vapor channels, which are less affected by the propagated error of the cloud properties. The statistics of the time series are summarized in terms of means and standard deviation for all data and for the data points only, which are consistent within the error bars (the numbers in parentheses in Fig. 3). The differences between the synthetic and observed satellite data are reduced for those data that passed the consistency check; for example, for the window channel at 10.8 μm the bias is reduced from 5 to 2 K and for the OLR it is reduced from 9 to 3.7 W m^{-2} in the mean values. Between 0000 and 0145 UTC as well as between 2000 and 0000 UTC, large discrepancies occur between the synthetic and observed satellite data that did not pass the consistency check. These discrepancies are analyzed next. Between 0000 and 0145 UTC, thin cirrus clouds passed the Lindenberg site. The ice water path (IWP) retrieved from the cloud radar is less than 14 g m^{-2} during this time period. The synthetic satellite observations are overestimated in the water-vapor channels at 6.2 and 7.3 μm as well as in the window channels (up to 30 K at 10.8 μm). Consistent with the overestimation of BT in these channels, the OLR of the synthetic satellite data is overestimated by up to 30 W m^{-2} as well. When clouds are present, the water-vapor channels contain information about the emission from water vapor above and within the clouds. In the presence of optically thin cirrus, the measurements also provide information on the water vapor below the clouds. In the case of an optically thick layer, the observed signals in the window channels 8.7, 10.8, and 12.0 μm are primary determined by the emission of radiation from the upper part of the cloud. In the case of semitransparent clouds, however, radiation emitted by the surface also influences the measurements at these wavelengths.

Because we are examining a semitransparent ice cloud between 0000 and 0145 UTC, the uncertainties in the simulated BTs are due to the uncertainties of the input surface parameter of the forward model, that is, the surface temperature and surface emissivity, and need to be taken into account. These uncertainties can only explain a 1-K uncertainty in the BTs as based on sensitivity studies assuming a 1-K uncertainty in the surface temperature and a 1% uncertainty in the surface emissivity. Thus the remaining overestimation of the synthetic BTs suggests that the CloudNET IWC used as input in RTTOV is underestimated and also suggests the uncertainty in the IWC. To quantify the potential underestimation of IWC, we performed sensitivity studies in which the IWC has been increased by factors from 2 up to 100. The best agreement between simulated and observed BTs, that is, BT difference of less than 0.5 K for all channels, has been found for a factor of 10. In this case, the mean IWP in this 2-h period is 35 g m^{-2}, implying that the cirrus is still transparent.

Between 2000 and 0000 UTC, the synthetic BTs of the water-vapor channels are underestimated by 5 K and they are overestimated in the other SEVIRI channels. The interpretation of these discrepancies is more difficult for several reasons. First, the cloud scene is more complex: after the precipitation event between 1740 and 1910 UTC, the ice clouds dissolve and low-level, broken clouds are present. While the cloud-phase detection algorithm from the satellite observations indicates liquid water, the ground-based CloudNET product identifies ice clouds most of the time. SEVIRI is not capable of detecting ice clouds or ice layers with relatively low ice water content overlying a water cloud or layer, which results in misclassification (Smith et al. 2008; Naud et al. 2005). Second, an underestimation of the IWC/LWC could explain the overestimation of the BTs in the window channels but not the underestimation in the water-vapor channels. To better explain these differences, we had a closer look at the development of the humidity profiles that are used as input to RTTOV and are provided by the COSMO-DE model. In addition, at the Lindenberg site radiosondes are accessible every 6 h. In particular, we compared the model profiles with

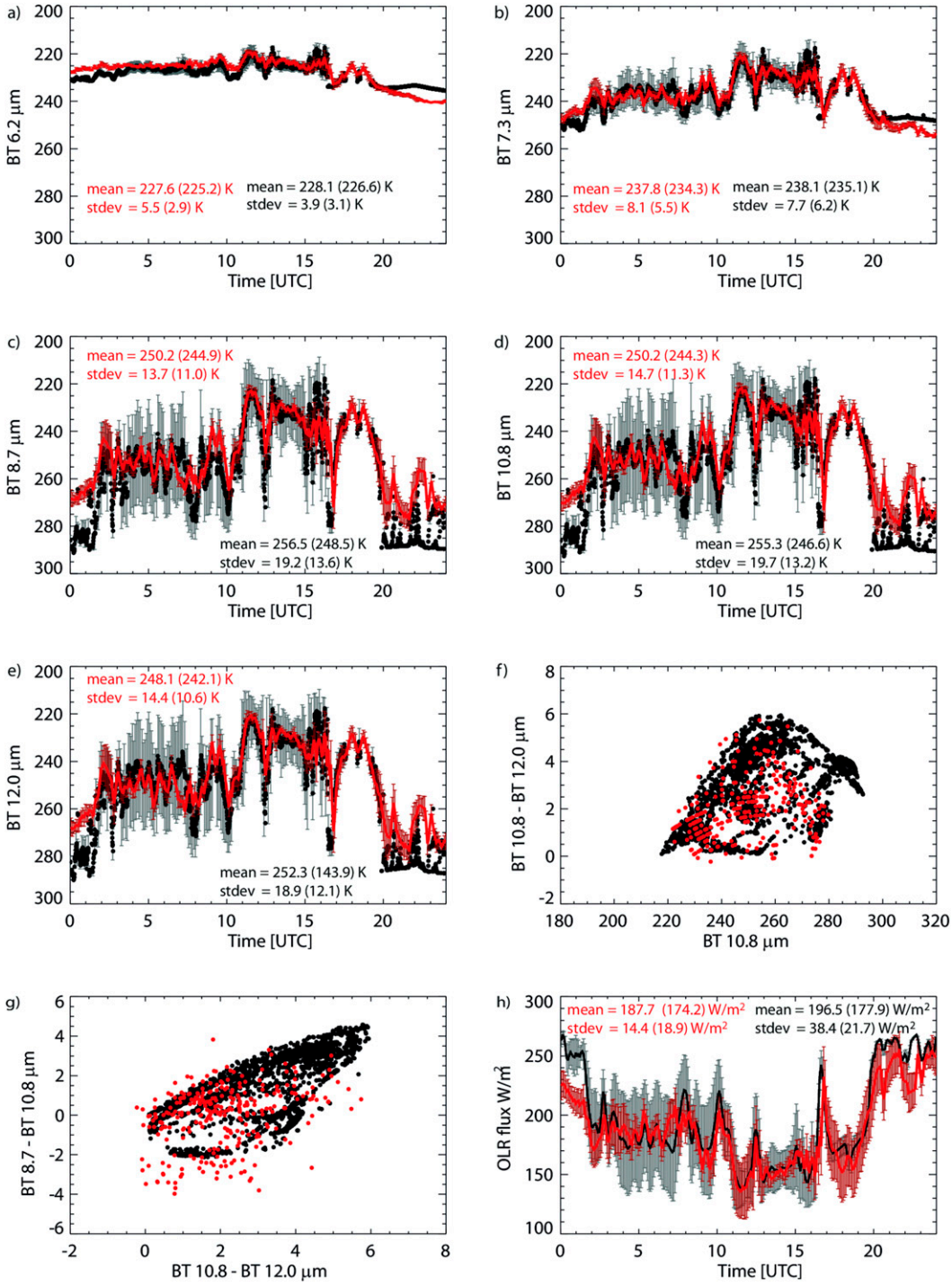

FIG. 3. Observed (red) and synthetic (black) brightness temperatures (K) on 12 May 2011 at Lindenberg. The error bars indicate the standard deviation of the 5×3 satellite pixels and the uncertainties of the CloudNET products, respectively. Shown are (a) BT6.2 μm, (b) BT7.3 μm, (c) BT8.7 μm, (d) BT10.8 μm, (e) BT12.0 μm, (f) split-window diagram (K), (g) trispectral diagram (K), and (h) OLR (W m^{-2}). Mean and standard deviation are calculated for all data and for only the data points that passed the consistency check (values in parentheses).

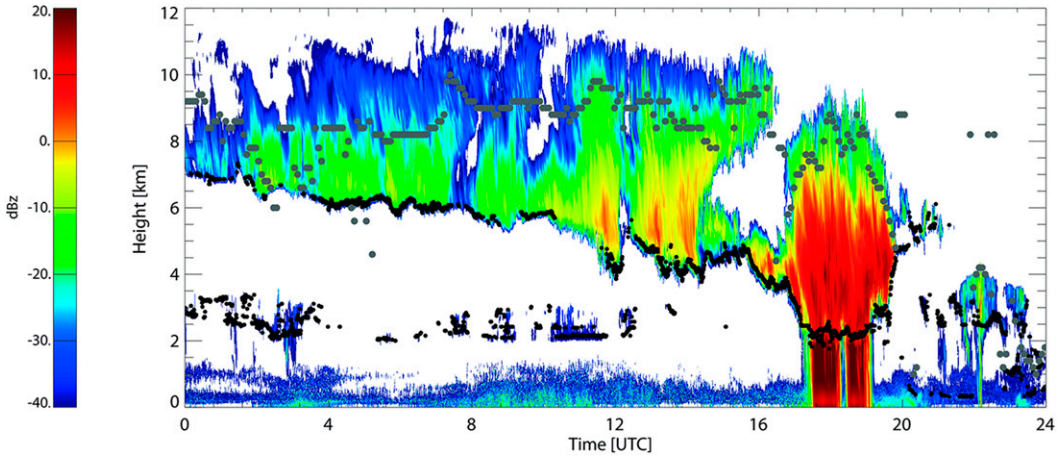

FIG. 4. Cloud-radar reflectivity at 30-s resolution from CloudNET on 12 May 2011 at Lindenberg with SEVIRI CTH (gray dots) and ceilometer cloud base (black dots).

radiosonde ascents at 1800 and 0000 UTC. It has been found that, for the 400–600-hPa layer, the COSMO-DE is 5 times as moist as the radiosonde at 0000 UTC. This overestimation of humidity can explain the discrepancy of the water-vapor channels, whereas for the window channels a combination of different parameters plays a role, for example, the diverse cloud-phase detection, surface temperature, and emissivity. In summary, the large discrepancies are dominated by low-level broken or thin cirrus clouds, which caused higher BTs and resulted in a lower mean and standard deviation (the numbers in parentheses in Fig. 3).

Differences between the BT at 10.8 and 12 μm versus 10.8 μm, referred to as the split-window technique, as well as the trispectral combination are widely used for detecting clouds and inferring cloud properties. These techniques are additionally used to understand the differences between the synthetic and observed satellite data. In the 12- and 8.7-μm channels, the optical properties are similar to those at 10.8 μm but the water absorptions are stronger and the emission of ice is changing. The split-window method shows the typical arc shape for the presence of clouds for the synthetic and observed satellite data that agree well (Fig. 3). In the trispectral technique, the difference BT8.7 − BT10.8 has positive values in the presence of cirrus clouds and is driven to negative differences for water clouds. Note that the observed satellite data show larger negative values than the synthetic satellite data in the trispectral technique, which belongs to the 2000–0000 UTC time period (Fig. 3). This result is caused by the different sensitivities of the ground- and satellite-based measurements due to the cloud phase.

b. *Characterization of the cloud system passing the station (Eulerian approach)*

Only those data that have passed the consistency check have been used in the following. The idea behind the check is to give us confidence to combine the cloud products from the satellite with the ones from the ground measurements to characterize the passing cloud systems over the site. Figure 4 presents the time series of the vertical profile of the radar reflectivity at the Lindenberg site together with the CTH retrieved from SEVIRI measurements and the cloud-base height provided by the ground-based ceilometer. The passing cold front is preceded by cirrostratus with intermittent altocumulus below. By 1600 UTC, the surface front passed Lindenberg, as can be identified by a minimum in the surface pressure and a drop in the surface temperature (not shown). Heavy rain with rain rates up to 9 mm h^{-1} occurred between 1740 and 1910 UTC after the passage of the surface front. Afterward, it cleared up, with 1–7 octal cumulus-cloud coverage. During the frontal passage, the wind turned from west to southwest and the cloud-base height of the upper cloud system decreased from 7 to 3 km while the cloud geometrical thickness grew from 1 to 7 km. The CTH increased from 8 to 11.8 km and decreased after the rain event. The CTH retrieved from the satellite data is too low because the satellite measurements are mainly sensitive to the extinction and hence the optical thickness of a cloud. Active instruments are suited to detect the vertical geometrical extent of a cloud and hence to detect the CTH.

The SEVIRI microphysical cloud products are only available during daytime and have been prepared as described in section 3a. Another cloud product that is available from both ground and satellite observations is the CWP. The SEVIRI CWP is compared with the sum of the CloudNET LWP and IWP, which is dominated by the ice phase. Only some low-level water clouds contribute to the CWP. The time series of the CWP retrieved from SEVIRI agrees very well with that of the

ground-based observations, with a correlation of 0.92 and a bias of 30.7 g m^{-2} (Fig. 5).

So far we have focused on understanding differences of the retrieved properties from both perspectives and have found that, for the periods that have passed the consistency test, the results agree very well. We now want to use disjunct cloud products to characterize the cloud system. At 0530 UTC, the cloud was semitransparent, having an optical thickness of 1.54, and that value increased to 13 at 1420 UTC (Fig. 6). Afterward, the COT decreased to 2 and increased again. The retrieved ice effective radius is 22 μm on average. The REF decreased from 27 μm at 0530 UTC to 12 μm at 1050 UTC, and increased again to 31 μm at 1205 UTC. During the latter time period (1050–1205 UTC), the variance of the Doppler velocities measured by the cloud radar increased in the upper layer of the cloud, which is an indication for higher atmospheric instability and a pronounced turbulent flux (Fig. 6). This situation can lead to the growth of ice particles as seen in the increase of REF. Note that these values are representative for the upper part of the cloud. The effective radius reached a maximum value of 38 μm at 1440 UTC. As broken multilayer clouds passed Lindenberg from 1500 to 1600 UTC the effective radius decreased. In Fig. 7 we used a different visualization to present the temporal evolution of COT and REF for the surrounding 5 × 3 pixels. This is useful to identify changes in the correlation pattern (positive and negative) and different cloud types. The temporal evolution of COT and REF is described by a triangular form. In the morning (0530–0900 UTC), a thin cirrostratus cloud with constant effective radius but slightly increasing COT persists. In the following period with mostly constant COT, ice particles grow. Thus the satellite-retrieved CWP increased in time (Fig. 5). Afterward, a broken multilayer cloud field reached Lindenberg with decreasing COT followed by decreasing REF. The approach of the cumulonimbus can be identified by an increase of the COT (red dots in Fig. 7). The altocumulus below the cirrostratus at 2–3-km height are also visible in Fig. 7 by the distinct lower REF and COT values.

c. *Characterization of the history of the cloud system (Lagrangian approach)*

To analyze the history of the cloud system, we have determined the origin of the air mass passing the supersite for four different states at the cloud frontal system: ahead of the front (0000 UTC), in the beginning of the front (0600 UTC), before the onset of precipitation (1200 UTC), and during the precipitation event (1800 UTC). The starting point for each trajectory is the Lindenberg observation site, and the CTH at

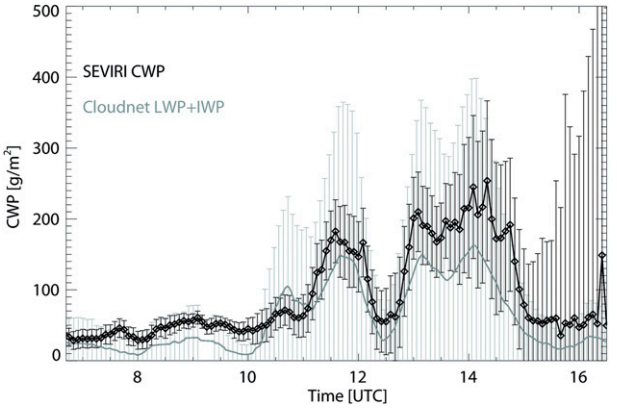

FIG. 5. The SEVIRI CWP (black line with diamonds) and the CloudNET CWP (gray line), which is the sum of IWP and LWP, between 0630 and 1630 UTC 12 May 2011 at Lindenberg. The vertical bars indicate the standard deviation of the 5 × 3 satellite pixels (black) and the uncertainties of the CloudNET cloud products (gray), respectively.

Lindenberg is used for the release of the tracked air particles. The averaged density tracks for each of the four times mentioned above are illustrated in Fig. 2. Each track has been calculated 24 h backward in time. The trajectories indicate that the cold-frontal system approached Lindenberg roughly from the southwest. The life times of the cloud systems are characterized by the cloud coverage, cloud phase, and CTH. The cloud coverage has been calculated from the binary cloud mask of the 5 × 3 surrounding pixels of the tracked air particles, which is used to characterize the horizontal inhomogeneity of the tracked cloud field (Fig. 8). The occurrence of each cloud phase (water and ice) at the top of the clouds has been computed for the 5 × 3 pixels along the track of the air parcel (Fig. 8).

In Fig. 9, the CTH of the tracked air particles is shown together with the standard deviation calculated from the CTH of the surrounding 5 × 3 pixels. Ahead of the front, the cloud cover is more variable as the track is at the edge of the frontal system. Note that full cloud coverage is observed along the back trajectories at later time steps lasting up to 14 h (e.g., at 1800 UTC starting time). As long as the cloud cover is 100%, the frontal system is characterized by a cirrus layer with a CTH of 10 km and a corresponding ice phase. Only for the 1800 UTC back trajectory, that is, during the precipitation event, is the CTH less than 10 km at the starting point. COT and REF along the 1800 UTC back trajectory are analyzed. The REF increased in the morning up to 37 μm with increasing COT. At 1200 UTC REF already decreased while COT increased (Fig. 10). A decrease in COT set in around 1300 UTC. To understand the decrease of the REF we used additional information from the German

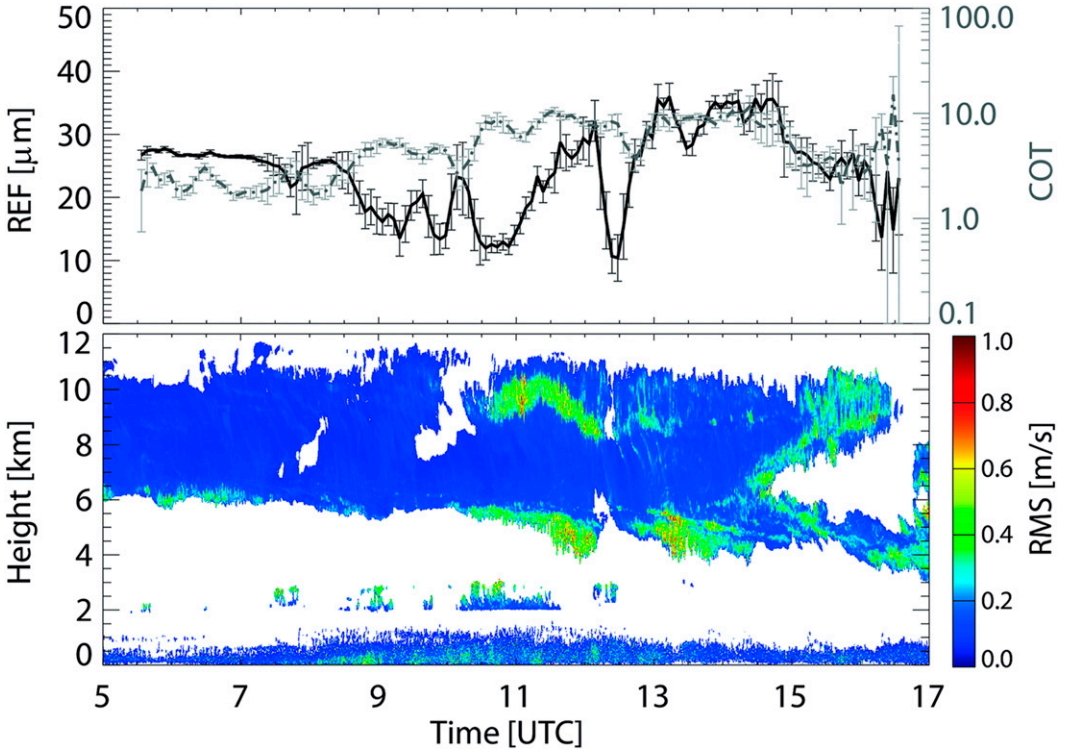

FIG. 6. (top) SEVIRI REF (black) and COT (gray) with the standard deviation of the 5 × 3 surrounding satellite pixels (vertical bars) and (bottom) the ground-based cloud-radar Doppler velocity between 0530 and 1630 UTC 12 May 2011 at Lindenberg.

Meteorological Service (Deutscher Wetterdienst) Radar-Online-Adjustment Network (DWD-RADOLAN) of precipitation radars to identify precipitation events along the track (DWD 2009). Several precipitation events occurred, with light rain at 1220 UTC and moderate-to-heavy rain at 1300 and 1340 UTC. During the precipitation events, the particle size at the top of the cloud has decreased, which might be explained by the sedimentation of large ice particles from the top of the cloud. The precipitation tends to reduce the correlation between COT and REF.

5. Summary and conclusions

A method has been introduced to study cloud frontal systems passing Europe. The combination of satellite- and ground-based observations and their comparison has been realized by utilizing the RTTOV model as a forward model to provide synthetic satellite data. We have used uncertainty estimates to characterize the temporal and spatial discrepancy of the ground- and satellite-based perspective. The uncertainties of the simulated BTs and measured BTs are related to the uncertainty estimates of the CloudNET cloud products and to the horizontal variation, respectively. Thereby we have established a consistency check, which builds the base for the study: If the synthetic satellite observations can reproduce the observed ones within the assumed uncertainties, we have confidence in both datasets from ground and space and can proceed with the analysis. We considered different metrics to quantify and interpret the consistency of the synthetic and the observed satellite data using brightness temperatures at the thermal IR

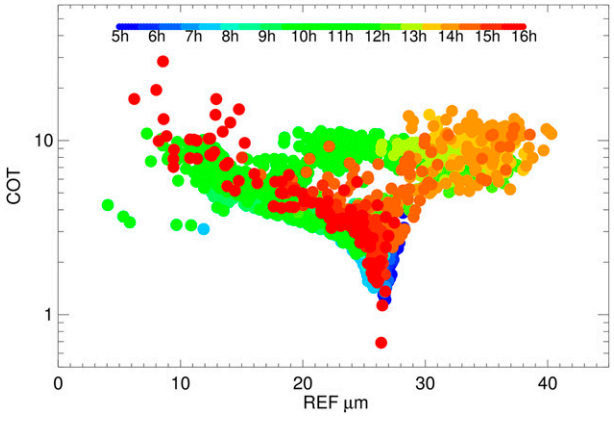

FIG. 7. SEVIRI cloud effective radius and COT at the parallax-corrected pixels with the surrounding 5 × 3 pixels on 12 May at Lindenberg. The colors indicate the time (UTC).

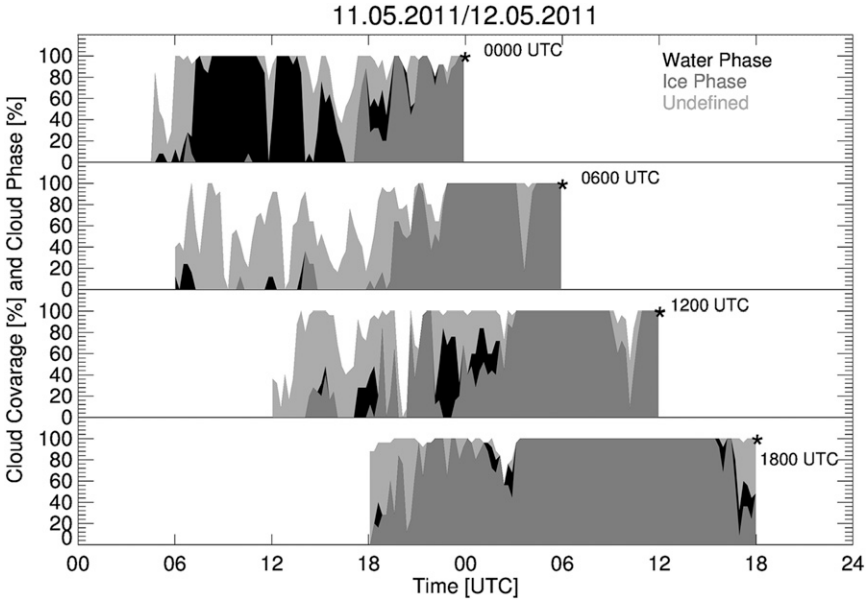

FIG. 8. SEVIRI cloud coverage and SEVIRI cloud phase (black: water; dark gray: ice; gray: undefined) for a cloud parcel that moved toward Lindenberg along the back trajectories for 0000, 0600, 1200, and 1800 UTC originating in Lindenberg (black stars) on 12 May 2011.

channels, the split-window channels, and trispectral combinations of channels as well as the outgoing longwave radiation.

Two periods were identified with significant differences between simulated and observed BTs that cannot be explained by the uncertainties. During the first period, the synthetic BTs and the OLR were overestimated relative to the observations. The analysis suggests an underestimation of the CloudNET IWC by as much as a factor of 10. The discrepancy observed during the second period likely results from multiple physical reasons, that is, from overestimation of the

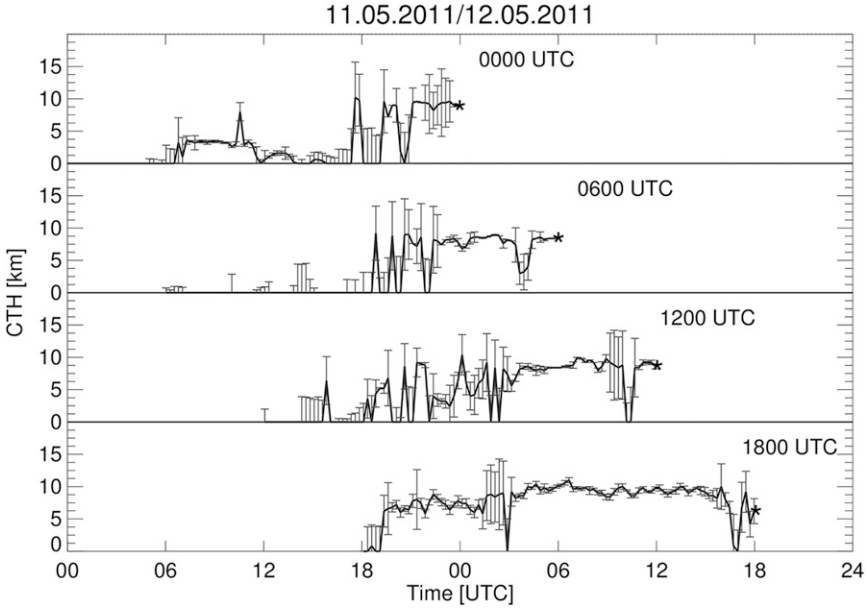

FIG. 9. SEVIRI CTH for a cloud parcel that moved toward Lindenberg along the back trajectories for 0000, 0600, 1200, and 1800 UTC originating in Lindenberg (black stars) on 12 May 2011. The vertical bars indicate the standard deviation determined from the 5×3 surrounding pixels.

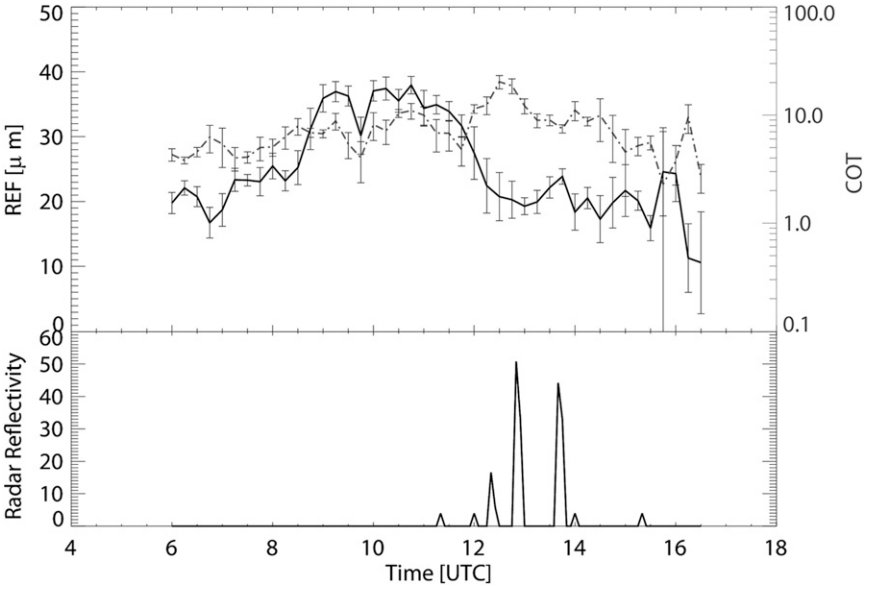

FIG. 10. (top) SEVIRI COT (gray line) and REF (black line) along the 1800 UTC back trajectory and (bottom) radar reflectivity (RADOLAN) along the 1800 UTC back trajectory.

forecast humidity profile, inhomogeneity of the cloud field, and the detection of different cloud phase. In summary, we have identified different sources of uncertainties that require further investigation: The IWC obtained from the CloudNET retrieval seems to underestimate the true ice water content, at least for the case studied here. This in turn leads to a significant overestimation of OLR and thus large discrepancies in the top-of-atmosphere radiation budget. A long-term study could reveal the frequency of such behavior and clarify its climatological relevance as well as provide guidance for the revision of IWC retrievals from cloud radar. An alternative approach could be the inclusion of satellite-observed BTs in the IWC retrieval as an additional constraint. The reason for the differences between the forecast humidity profile and the radiosoundings are also unclear and might be connected to a precipitation event. The results of our comparison are used to assess the uncertainties of the individual observations. On the basis of both ground- and satellite-based datasets, we obtained an overview of the different cloud properties to get a three-dimensional cloud field, including its uncertainties. For this case study, the comparison of the satellite-based CWP and CloudNET-derived IWP/LWP shows good agreement, which suggests that the satellite products provide valuable information for the cloud types studied, despite their relatively large uncertainties.

After the successful consistency check, the different states during the life cycle of the cloud system have been investigated by adopting both the Euler and Lagrange reference frames. The Eulerian approach has been used to analyze the cloud system as it passes over the ground station. The various states of the cloud system starting from optical thin high-top clouds to low-top clouds, multilayer clouds as well as precipitation have been identified and analyzed with respect to the physical properties of the cloud system. The combination of the ground-based observations, specifically the Doppler velocity, with the cloud effective radius has enabled new insights into the microphysical processes of the clouds. The demonstration of the described method motivates the realization of further studies that might form a more statistical basis to the analysis of frontal systems passing Europe supersites. The analysis would include classification in different weather regimes. One focus could be on the understanding of the relation between REF and COT, as well as OLR related to cloud processes, retrieved from the ground-based observation. In addition, the horizontal variation given by the standard deviation at the window channel has not been investigated so far and should be further analyzed.

The recent increase in the number of cloud-radar observations throughout Europe allows us to extend our approach from one point measurement to a network offering temporally and vertically resolved observations. The Lagrangian approach adopted here not only provides the history of the cloud systems approaching these measurement sites but also allows us to link observations between the sites. By following the cloud parcel with SEVIRI, the evaluation of the horizontal

structure of the cloud field, the cloud-top height, and the microphysical cloud properties can be studied on the track, but the changes of the vertical profile to the next site with respect to the travel time can also be studied.

Acknowledgments. This work has been funded by the German Research Foundation within the project Integrating Cloud Observations from Ground and Space (ICOS) under Grant CR111/8-1. We acknowledgment the EUMETSAT SAFS for providing the SEVIRI cloud products as well as the CloudNET project (European Union Contract EVK2-2000-00611) for providing the ground-based cloud products, which were produced by the German Weather Service using measurements from Lindenberg. We thank the reviewers for their valuable comments.

REFERENCES

Albrecht, B. A., C. W. Fairall, D. W. Thomson, A. B. White, J. B. Snider, and W. H. Schubert, 1990: Surface-based remote sensing of the observed and the adiabatic liquid water content of stratocumulus clouds. *Geophys. Res. Lett.,* **17,** 89–92, doi:10.1029/GL017i001p00089.

Astin, I., L. Di Girolamo, and H. M. Poll, 2001: Bayesian confidence intervals for true fractional coverage from finite transect measurements: Implications for cloud studies from space. *J. Geophys. Res.,* **106,** 17 303–17 310, doi:10.1029/2001JD900168.

Bjerknes, J., 1919: On the structure of moving cyclones. *Mon. Wea. Rev.,* **47,** 95–99, doi:10.1175/1520-0493(1919)47<95:OTSOMC>2.0.CO;2.

Boers, R., H. Russchenberg, J. Erkelens, V. Venema, A. van Lammeren, A. Apituley, and S. Jongen, 2000: Ground-based remote sensing of stratocumulus properties during CLARA, 1996. *J. Appl. Meteor.,* **39,** 169–181, doi:10.1175/1520-0450(2000)039<0169:GBRSOS>2.0.CO;2.

Bouniol, D., and Coauthors, 2010: Using continuous ground-based radar and lidar measurements for evaluating the representation of clouds in four operational models. *J. Appl. Meteor. Climatol.,* **49,** 1971–1991, doi:10.1175/2010JAMC2333.1.

Deneke, H., W. Knap, and C. Simmer, 2009: Multiresolution analysis of the temporal variance and correlation of transmittance and reflectance of an atmospheric column. *J. Geophys. Res.,* **114,** D17206, doi:10.1029/2008JD011680.

Derrien, M., 2012: Validation report for "cloud products" (CMa-PGE01 v3.2, CT-PGE02 v2.2 & CTTH-PGE03 v2.2). NWC SAF Tech. Rep. SAF/NWC/CDOP/MFL/SCI/VR/06, 31 pp. [Available online at http://www.nwcsaf.org/scidocs/Documentation/SAF-NWC-CDOP-MFL-SCI-VR-06_v1.0.pdf.]

——, 2013: Algorithm theoretical basis document for "cloud products" (CMa-PGE01 v3.2, CT-PGE02 v2.2 & CTTH-PGE03 v2.2). NWC SAF Tech. Rep. SAF/NWC/CDOP2/MFL/SCI/ATBD/01, Issue 3, Rev. 2.1, 87 pp. [Available online at http://www.nwcsaf.org/HTMLContributions/SUM/SAF-NWC-CDOP2-MFL-SCI-ATBD-01_v3.2.1.pdf.]

DWD, 2009: RADOLAN-RADVOR-OP: Beschreibung des Kompositformats, version 2.2.1. Deutscher Wetterdienst Tech. Rep., 19 pp. [Available online at http://www.dwd.de/bvbw/generator/DWDWWW/Content/Wasserwirtschaft/en/Unsere__Leistungen__en/Radarniederschlagsprodukte__en/RADOLAN__en/RADOLAN__RADVOR__OP__Komposit__format__2__2__1__pdf,templateId=raw,property=publicationFile.pdf/RADOLAN_RADVOR_OP_Komposit_format_2_2_1_pdf.pdf.]

EUMETSAT, 2014: Outgoing longwave radiation product: Factsheet. EUMETSAT Tech. Doc. EUM/OPS/DOC/09/5176, issue v1D, 10 pp. [Available online at http://www.eumetsat.int/website/wcm/idc/idcplg?IdcService=GET_FILE&dDocName=PDF_OLR_FACTSHEET&RevisionSelectionMethod=LatestReleased&Rendition=Web.]

Eyre, J., 1991: A fast radiative transfer model for satellite sounding systems. ECMWF Internal Tech. Memo. 176, 28 pp. [Available online at http://old.ecmwf.int/publications/library/ecpublications/_pdf/tm/001-300/tm176.pdf.]

Feijt, A., and A. van Lammeren, 1996: Ground-based and satellite observations of cloud fields in the Netherlands. *Mon. Wea. Rev.,* **124,** 1914–1923, doi:10.1175/1520-0493(1996)124<1914:GBASOO>2.0.CO;2.

Field, P. R., and R. Wood, 2007: Precipitation and cloud structure in midlatitude cyclones. *J. Climate,* **20,** 233–254, doi:10.1175/JCLI3998.1.

——, A. Gettelman, R. Neale, R. Wood, P. Rasch, and H. Morrison, 2008: Midlatitude cyclone compositing to constrain climate model behavior using satellite observations. *J. Climate,* **21,** 5887–5903, doi:10.1175/2008JCLI2235.1.

——, A. Bodas-Salcedo, and M. Brooks, 2011: Using model analysis and satellite data to assess cloud and precipitation in midlatitude cyclones. *Quart. J. Roy. Meteor. Soc.,* **137,** 1501–1515, doi:10.1002/qj.858.

Greuell, W., and R. Roebeling, 2009: Toward a standard procedure for validation of satellite-derived cloud liquid water path: A study with SEVIRI data. *J. Appl. Meteor. Climatol.,* **48,** 1575–1590, doi:10.1175/2009JAMC2112.1.

Grützun, V., J. Quaas, C. Morcrette, and F. Ament, 2013: Evaluating statistical cloud schemes: What can we gain from ground-based remote sensing? *J. Geophys. Res. Atmos.,* **118,** 10 507–10 517, doi:10.1002/jgrd.50813.

Higgins, C. W., M. Froidevaux, V. Simeonov, N. Vercauteren, C. Barry, and M. B. Parlange, 2012: The effect of scale on the applicability of Taylor's frozen turbulence hypothesis in the atmospheric boundary layer. *Bound.-Layer Meteor.,* **143,** 379–391, doi:10.1007/s10546-012-9701-1.

Hogan, R. J., M. P. Mittermaier, and A. J. Illingworth, 2006: The retrieval of ice water content from radar reflectivity factor and temperature and its use in evaluating a mesoscale model. *J. Appl. Meteor. Climatol.,* **45,** 301–317, doi:10.1175/JAM2340.1.

Illingworth, A. J., and Coauthors, 2007: Cloudnet: Continuous evaluation of cloud profiles in seven operational models using ground-based observations. *Bull. Amer. Meteor. Soc.,* **88,** 883–898, doi:10.1175/BAMS-88-6-883.

Jakob, C., 2003: An improved strategy for the evaluation of cloud parameterizations in GCMs. *Bull. Amer. Meteor. Soc.,* **84,** 1387–1402, doi:10.1175/BAMS-84-10-1387.

McFarquhar, G. M., S. Iacobellis, and R. C. Somerville, 2003: SCM simulations of tropical ice clouds using observationally based parameterizations of microphysics. *J. Climate,* **16,** 1643–1664, doi:10.1175/1520-0442(2003)016<1643:SSOTIC>2.0.CO;2.

Nakajima, T., and M. D. King, 1990: Determination of the optical thickness and effective particle radius of clouds from reflected solar radiation measurements. Part I: Theory. *J. Atmos.*

Sci., **47,** 1878–1893, doi:10.1175/1520-0469(1990)047<1878:DOTOTA>2.0.CO;2.

Naud, C. M., J.-P. Muller, and P. De Valk, 2005: On the use of ICESAT-GLAS measurements for MODIS and SEVIRI cloud-top height accuracy assessment. *Geophys. Res. Lett.,* **32,** L19815, doi:10.1029/2005GL023275.

——, A. D. Del Genio, M. Bauer, and W. Kovari, 2010: Cloud vertical distribution across warm and cold fronts in *CloudSat–CALIPSO* data and a general circulation model. *J. Climate,* **23,** 3397–3415, doi:10.1175/2010JCLI3282.1.

Roebeling, R., A. Feijt, and P. Stammes, 2006: Cloud property retrievals for climate monitoring: Implications of differences between spinning enhanced visible and infrared imager (SEVIRI) on *METEOSAT-8* and Advanced Very High Resolution Radiometer (AVHRR) on *NOAA-17*. *J. Geophys. Res.,* **111,** D20210, doi:10.1029/2005JD006990.

——, H. Deneke, and A. Feijt, 2008: Validation of cloud liquid water path retrievals from SEVIRI using one year of CloudNET observations. *J. Appl. Meteor. Climatol.,* **47,** 206–222, doi:10.1175/2007JAMC1661.1.

Saunders, R. W., M. Matricardi, and P. Brunel, 1999: An improved fast radiative transfer model for assimilation of satellite radiances observations. *Quart. J. Roy. Meteor. Soc.,* **125,** 1407–1425, doi:10.1256/smsqj.55614.

——, ——, and A. Geer, 2010: RTTOV-9 users guide. EUMETSAT Tech. Rep. NWPSAF-MO-UD-016, 57 pp. [Available online at http://nwpsaf.eu/deliverables/rtm/rttov9_files/users_guide_9_v1.7.pdf.]

Schmetz, J., P. Pili, S. Tjemkes, D. Just, J. Kerkmann, S. Rota, and A. Ratier, 2002: An introduction to Meteosat Second Generation (MSG). *Bull. Amer. Meteor. Soc.,* **83,** 977–992, doi:10.1175/1520-0477(2002)083<0977:AITMSG>2.3.CO;2.

Schulz, J., and Coauthors, 2009: Operational climate monitoring from space: The EUMETSAT Satellite Application Facility on Climate Monitoring (CM-SAF). *Atmos. Chem. Phys.,* **9,** 1687–1709, doi:10.5194/acp-9-1687-2009.

Shapiro, M. A., and S. Grønås, 1999: *The Life Cycles of Extratropical Cyclones.* Amer. Meteor. Soc., 359 pp.

Smith, W. L., P. Minnis, H. Finney, R. Palikonda, and M. M. Khaiyer, 2008: An evaluation of operational GOES-derived single-layer cloud top heights with ARSCL data over the ARM Southern Great Plains site. *Geophys. Res. Lett.,* **35,** L13820, doi:10.1029/2008GL034275.

Stephens, G. L., 1978: Radiation profiles in extended water clouds. II: Parameterization schemes. *J. Atmos. Sci.,* **35,** 2123–2132, doi:10.1175/1520-0469(1978)035<2123:RPIEWC>2.0.CO;2.

——, and Coauthors, 2002: The *CloudSat* mission and the A-Train. *Bull. Amer. Meteor. Soc.,* **83,** 1771–1790, doi:10.1175/BAMS-83-12-1771.

Stohl, A., C. Forster, A. Frank, P. Seibert, and G. Wotawa, 2005: Technical note: The Lagrangian particle dispersion model FLEXPART version 6.2. *Atmos. Chem. Phys.,* **5,** 2461–2474, doi:10.5194/acp-5-2461-2005.

Stokes, G. M., and S. E. Schwartz, 1994: The Atmospheric Radiation Measurement (ARM) Program: Programmatic background and design of the cloud and radiation test bed. *Bull. Amer. Meteor. Soc.,* **75,** 1201–1221, doi:10.1175/1520-0477(1994)075<1201:TARMPP>2.0.CO;2.

Taylor, G. I., 1938: The spectrum of turbulence. *Proc. Roy. Soc. London,* **164A,** 476–490, doi:10.1098/rspa.1938.0032.

van Lammeren, A., A. Feijt, J. Konings, E. van Meijgaard, and A. Van Ulden, 2000: Combination of ground-based and satellite cloud observations on a routine basis. *Meteor. Z.,* **9,** 125–134.

Wan, Z., D. Ng, and J. Dozier, 1994: Spectral emissivity measurements of land-surface materials and related radiative transfer simulations. *Adv. Space Res.,* **14,** 91–94, doi:10.1016/0273-1177(94)90197-X.

Winker, D. M., M. A. Vaughan, A. Omar, Y. Hu, K. A. Powell, Z. Liu, W. H. Hunt, and S. A. Young, 2009: Overview of the *CALIPSO* mission and CALIOP data processing algorithms. *J. Atmos. Oceanic Technol.,* **26,** 2310–2323, doi:10.1175/2009JTECHA1281.1.

Zinner, T. and B. Mayer, 2006: Remote sensing of stratocumulus clouds: Uncertainties and biases due to inhomogeneity. *J. Geophys. Res.,* **111,** D14209, doi:10.1029/2005JD006955.